



Suitability of artificial bulk viscosity for large-eddy simulation of turbulent flows with shocks

Ali Mani *, Johan Larsson, Parviz Moin

Center for Turbulence Research, Stanford University, Stanford, CA 94305, United States

ARTICLE INFO

Article history:

Received 3 December 2008

Received in revised form 25 June 2009

Accepted 28 June 2009

Available online 10 July 2009

Keywords:

Shock–turbulence interaction

Large-eddy simulation

Compressible flow

Artificial bulk viscosity

Sound prediction

ABSTRACT

The artificial bulk viscosity method to numerically capture shocks is investigated for large-eddy simulation (LES). Different variations of this method are tested on a turbulent flow over a cylinder at Reynolds number of 10,000 and free-stream Mach number of 0.85. The artificial bulk viscosity model by Cook and Cabot, which is parameterized by the strain rate magnitude, is found to provide unnecessary bulk viscosity in turbulent regions away from shocks. While developed turbulent structures are found unaffected, this extra bulk viscosity is shown to significantly damp the sound field. An alternative formulation of the model which is parameterized by the rate of dilatation is proposed. This formulation is shown to avoid the unnecessary bulk viscosity and enhance the sound-prediction capability of the model. It was found that standard LES combined with artificial bulk viscosity is a promising approach for simulation of turbulent flows with shocks. The formulation of the model on curvilinear coordinates is presented in the appendix.

© 2009 Elsevier Inc. All rights reserved.

1. Introduction

While the literature includes many robust and accurate numerical methods for the computation of shock waves or turbulence, the simultaneous prediction of these phenomena remains a challenge. Capturing an essentially discontinuous shock wave on a realistic grid requires the addition of numerical viscosity that scales as $\mu_{\text{num}} \sim \rho \delta u \Delta$, where δu is the velocity jump across the shock, Δ is some characteristic grid spacing, and ρ is density. Turbulence, on the other hand, presents a completely different set of requirements. It has been shown that even high-order dissipative numerics significantly damp turbulence in a broad range of wavenumbers [1,2]. This is particularly important in the framework of large-eddy simulation (LES), where even the smallest resolved structures carry dynamically valuable information. Thus, the inherently conflicting requirements of computing shock/turbulence interactions are clear: The amount of dissipation required for shock capturing may cause underprediction of turbulent fluctuations.

One interesting approach for shock treatment was used by Shebalin [3] and then improved to an adaptive form by Cook and Cabot [4]. The key idea in these studies was to provide dissipation to the dilatational velocity field without directly affecting (dissipating) the vortical velocity field. Consider the viscous stress tensor

$$\tau_{ij} = \mu \left(\frac{\partial u_i}{\partial x_j} + \frac{\partial u_j}{\partial x_i} - \frac{2}{3} \frac{\partial u_k}{\partial x_k} \delta_{ij} \right) + \beta \frac{\partial u_k}{\partial x_k} \delta_{ij},$$

where \mathbf{u} is the velocity field and μ and β are the shear and bulk viscosities, respectively. Cook and Cabot [4] augmented the physical bulk viscosity, β , by an artificial bulk viscosity (ABV)

* Corresponding author. Tel.: +1 650 723 9548.

E-mail address: alimani@stanford.edu (A. Mani).

$$\beta_{\Delta} \sim \rho \Delta^{(2r+2)} \overline{|\nabla^{2r} S|}, \quad (1)$$

where $S = \sqrt{S_{ij}S_{ij}}$ is the magnitude of the strain rate tensor, ∇^{2r} is a series of r Laplacians, and the overbar denotes a wide Gaussian filter to remove high wavenumber oscillations introduced by the Laplacians and the absolute value operator. This ABV scales as $\sim \rho \delta u \Delta$ at shocks; therefore, it diffuses them over a few grid spacings Δ . The purpose of the Laplacians, i.e., having $r > 0$, is to localize the ABV to rapidly varying regions of the flow.

We note that a similar augmentation of the shear viscosity, μ , can provide shock capturing, but this would directly dissipate vortical structures as well. An augmented bulk viscosity, on the other hand, does not directly affect vortical motions. To demonstrate this, consider the effect of the ABV term on the vorticity equation

$$\frac{d\omega}{dt} = RHS_1 - \frac{\nabla \rho}{\rho^2} \times \nabla [\beta_{\Delta} (\nabla \cdot \mathbf{u})],$$

where ω is vorticity, d/dt represents the material derivative, and RHS_1 is the physical right-hand-side of the vorticity equation. It is clear that the ABV does not lead to a diffusive term in this equation. In addition, the term is expected to be small both near and away from shocks. Near shocks, the gradients of both ρ and $\beta_{\Delta} (\nabla \cdot \mathbf{u})$ are parallel, and therefore their cross product is small. In turbulent regions away from shocks, dilatational fluctuations are small (relative to the vorticity), thus making the term small. It is this property of having a minimal effect on the vorticity field that makes the ABV method a good candidate for shock/turbulence interaction problems. However, it will be shown below that the ABV has a non-negligible effect on the dilatational motions: this is what the proposed modifications in this study are intended to improve upon.

The first purpose of this paper is to assess the performance of the ABV method when applied to complex turbulent flows involving shocks. Transonic turbulent flow over a cylinder is considered as a platform to test this method when combined with LES. Complex features of this flow includes shock/turbulence interactions, shock/wall interactions, transition to turbulence, and sound generation.

Although ABV minimally affects vortical structures, it can have a significant impact on sound predictions. This can be seen by considering the dilatation equation

$$\frac{d(\nabla \cdot \mathbf{u})}{dt} = RHS_2 + \nabla \cdot \left[\frac{1}{\rho} \nabla [\beta_{\Delta} (\nabla \cdot \mathbf{u})] \right],$$

where RHS_2 represents the physical right-hand side of the dilatation equation. The ABV gives rise to a diffusive term with a diffusion coefficient that scales as β_{Δ}/ρ . Hence, the ABV term damps dilatational motions: this is the intended purpose at shocks, but it can also lead to an unphysical damping of the generated sound field. Therefore, it is important to limit the presence of this term only to shock-containing regions. The second purpose of this paper is to propose some simple modifications to the ABV method that minimizes β_{Δ} away from shocks. In Section 3 these modifications will be shown to significantly enhance the sound-prediction capability of LES where the ABV method is used for shock capturing.

2. Proposed improvements

The first proposed improvement to the ABV model is to replace the strain-rate magnitude S in Eq. (1) by the dilatation $\nabla \cdot \mathbf{u}$. It is straightforward to see that $|\nabla \cdot \mathbf{u}| \approx S$ at shock waves, and hence this modification does not alter the shock-capturing capability of the method. Turbulence, on the other hand, is inherently vortical, and thus $|\nabla \cdot \mathbf{u}| \ll S$; therefore the modification should significantly decrease the ABV in turbulent regions.

The second proposed improvement is to “turn off” the ABV in regions where the fluid is expanding, which is accomplished by including the Heaviside function $H(-\nabla \cdot \mathbf{u})$ in the definition of β_{Δ} . The purpose of the ABV is to capture shocks, and there is no reason to add an artificial (and inherently unphysical) property where shocks cannot occur.

The final proposed improvement is to take the length scale Δ as the grid spacing normal to the shock, which ensures consistent shock capturing regardless of the local orientation and anisotropy of the grid; this is not the case for the extension to curvilinear grids in Ref [5]. In addition, the present formulation removes the common ambiguity regarding the choice of a length scale on anisotropic and/or curvilinear grids. We therefore define the final model as

$$\beta_{\Delta} = C \rho \overline{D^{2r}(\nabla \cdot \mathbf{u})} |H(-\nabla \cdot \mathbf{u})|, \quad (2)$$

where the operator $D^{2r}(\cdot)$ is defined in the Appendix to mimic $\Delta^{(2r+2)} \nabla^{2r}(\cdot)$ on curvilinear grids, but with a length scale that is equal to the grid spacing normal to the shock. The filter operator in Eq. (2) is the same as the one used by Cook and Cabot [4], except that it here acts on the entire term to yield a smoother β_{Δ} .

In this paper we consider three variants of the ABV, as listed in Table 1. Case A is close to the formulation by Cook and Cabot [4], but with the proposed definitions of Δ and D^{2r} for curvilinear grids (which we need in the present test case) and the Heaviside function that switches off the ABV in expansion regions (for a fair comparison). We use the same model constant $C = 1.0$ and order $r = 2$ as recommended in Ref. [4]. Case B is the proposed method given by Eq. (2), with identical C and r . Comparing Cases A and B therefore shows the effect of replacing S by $\nabla \cdot \mathbf{u}$; as shown below this significantly enhances the generation of sound.

Table 1

Summary of different ABV models investigated in LES of the flow over a cylinder.

	Form of ABV	r	C	Description
Case A	$D^4(S)$	2	1.0	High order based on S
Case B	$D^4(\nabla \cdot \mathbf{u})$	2	1.0	High order based on $\nabla \cdot \mathbf{u}$
Case C	$D^0(\nabla \cdot \mathbf{u})$	0	3.25	Low order based on $\nabla \cdot \mathbf{u}$

These parameters are used in Eqs. (3) and (4) which describe the curvilinear extension of Eq. (2).

We finally consider the effect of the order parameter r . On otherwise smooth problems a higher value of r should improve the localization of the ABV to regions of shocks. In LES, however, the vorticity field is under-resolved and high-wavenumber oscillations are present everywhere; in such regions, the effect of the Laplacians is unclear. In Case C we therefore remove the Laplacians to investigate this effect. The constant C is tuned such that it gives the same shock thickness as Cases A and B for a weak 1D shock. We point out that $r = 0$ is used solely for testing, and is not generally recommended since it would not lead to satisfactorily small β_A in certain cases (e.g., isentropic compression or sound propagation).

3. LES of transonic flow over a cylinder

We solve the compressible Navier–Stokes equations for a perfect gas with gas constant $\gamma = 1.4$ and Prandtl number $Pr = 0.7$, and use ABV for shock capturing. Cook and Cabot [4] proposed an artificial shear viscosity to account for the unresolved vortical motions. In the present work, however, we instead use the dynamic Smagorinsky model of Moin et al. [6] with the modification of Lilly [7] to determine the subgrid-scale shear viscosity (μ_A) and the subgrid-scale thermal diffusivity. The dynamic model has been successfully validated in numerous LES calculations of separated flows, including many cylinder flows. This is not the case for the artificial shear viscosity. By using the well-known dynamic Smagorinsky model we, therefore, limit the number of unknown parameters in the tests.

The equations are solved for flow over a cylinder at Reynolds number of 10,000 and Mach number of 0.85, on a curvilinear staggered grid using a sixth-order LES code [8]. The spatial discretization is fully conservative and uses compact finite differences. The time advancement scheme is second-order implicit near the cylinder wall and third-order Runge-Kutta away from the wall. More details on the numerical scheme are presented in Ref. [8], and validation test cases for the flow over a cylinder at different conditions can be found in Ref. [9].

The computational domain has a radius of approximately $35D$ ($D =$ cylinder diameter) and a width of πD in the spanwise direction. The mesh size is $513 \times 360 \times 40$ in the wall normal, azimuthal, and spanwise directions, respectively, totaling about 7.4 million grid points. The wall normal grid spacing at the leading edge is $0.00124D$ with a maximum grid stretching of 4%. A “sponge” layer with a thickness of $15D$ is applied at the outer boundary to damp unsteady flow features exiting the domain and making the boundary non-reflecting. The time step for all ABV cases is equal to $3.1 \times 10^{-3}D/c_\infty$. After ensuring that any initial transients have disappeared, data is collected over 80 time units tU_∞/D (about 16 shedding cycles). The results on this grid are compared to a refined calculation with a refinement factor of two in both time-step and grid-spacings in all directions. The ABV model in Case C was used for the refinement study.

Fig. 1 shows an instantaneous picture of the flow. There are weak oblique shocks where the laminar boundary layers separate, and stronger almost normal shocks around $x \approx 4D$. The initially laminar wake transitions to turbulence around $x \approx 2D$.

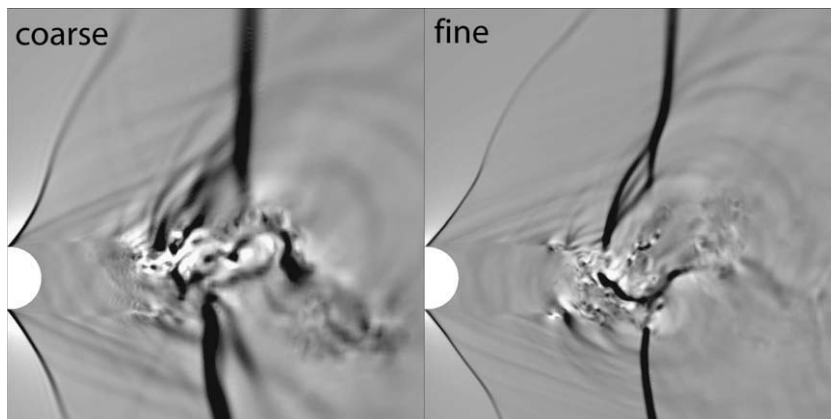


Fig. 1. Instantaneous dilatation fields on the coarse and fine grids, with contour levels between $\pm c_\infty/D$. Note that the snapshots represent two different realizations.

The turbulent wake generates sound which propagates to the far field. As expected, the fine-grid results show sharper features and a higher level of detail.

Fig. 2 shows the average artificial bulk viscosities. All cases yield similar levels of ABV at the shocks, which is to be expected since $|\nabla \cdot \mathbf{u}| \approx S$ there. However, in the wake region away from the shocks, there are significant differences between the models. Going from Case A to Case B reduces the ABV by a factor of about 5 on the wake centerline, and Case C brings an additional factor of 5 reduction. To interpret this difference, note that the shocks outside the wake region exist at all times, whereas there are only shocklets inside the wake region intermittently. Therefore, the average ABV should be lower in the wake region than at the shocks. The reason for the large levels of ABV in the wake region of Case A is that this model operates on the strain rate magnitude S , which is both large and rapidly varying in the turbulent wake region; the dilatation $\nabla \cdot \mathbf{u}$ is much smaller in turbulence, leading to the lower levels of ABV in Case B. Finally, the further decrease of ABV in Case C clearly shows that the effect of the Laplacians can be counter-intuitive in turbulent regions.

Fig. 3 shows snapshots of the dilatation field, where it is clear that the cases with lower ABV radiate more sound. This is quantified in Fig. 4, which shows the far-field sound spectra. Cases B and C agree with the fine-grid spectrum for frequencies up to about $4\omega_{\text{shedding}}$. In contrast, Case A underpredicts the far-field sound by a factor of about 4 across a wide range of frequencies. To interpret these results, one must first note that the far-field sound is generated in the turbulent wake region and then propagates to the far field. Since $|\nabla \cdot \mathbf{u}| \approx S$ in a sound wave, the Cases A and B treat the propagation of sound waves similarly. Therefore, the difference in the far-field sound between these two cases must stem from the generation of sound, which takes place in the wake region. This is where Case A introduces significant artificial bulk viscosity as shown in Fig. 2.

Next we consider a comparison between Cases B and C. The far-field sound is similar at low to medium frequencies, despite Case C showing lower levels of ABV in the sound generation region (Fig. 2). Therefore, there appears to be a critical level below which further reduction in the ABV makes little difference on the turbulent dilatational motions. The lower sound level of Case C at high frequencies is due to lack of Laplacian operators in Case C which fails to deactivate the ABV in the smooth sound propagation region. This illustrates why at least one Laplacian is needed, i.e., $r \geq 1$ is recommended for general flows. Overall, most of the improvement is due to replacing S by $\nabla \cdot \mathbf{u}$, whereas the order parameter r has a smaller effect.

We finally consider the spectra of vertical velocity at the three locations shown in Fig. 5. Comparison of these spectra shows how the prediction of turbulent structures can be affected by the ABV model. At the fully turbulent locations ($x = 3D$ and $5D$) the spectra from all cases agree well. A similar observation was made for the spectra of other velocity components. The agreement of different models in fully turbulent regions shows that vortical structures are not affected by excessive ABV in model A. However, at $x = 2D$ Case A yields a lower spectrum by a factor ~ 3 across a wide range of frequencies. While the precise reason of this trend is unclear and subject to further investigations, the following appears to be a plausible explanation:

The wake flow has not fully transitioned to turbulence at $x = 2D$ as evident by the lower spectral energy levels. Therefore, the relative strength of dilatational modes in this region and excessive damping of dilatation by model A can explain the underprediction of velocity fluctuations at $x = 2D$. Note that the plots of spectra are shown in log-scale; same error at $x = 3D$ is less apparent due to higher level of vorticity, and thus spectral energy.

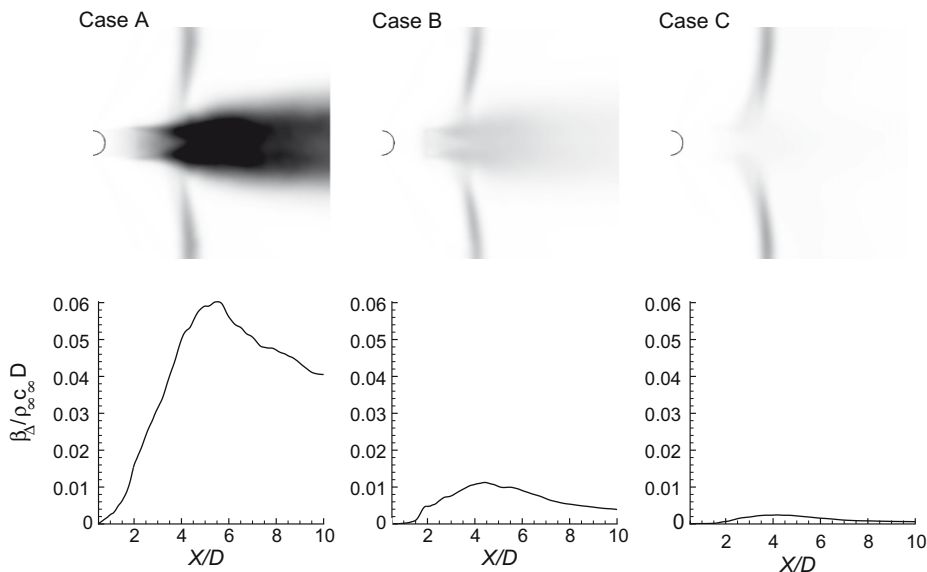


Fig. 2. Average ABV fields (top row) for the different methods listed in Table 1. The bottom row shows the average values in the wake along the centerline.

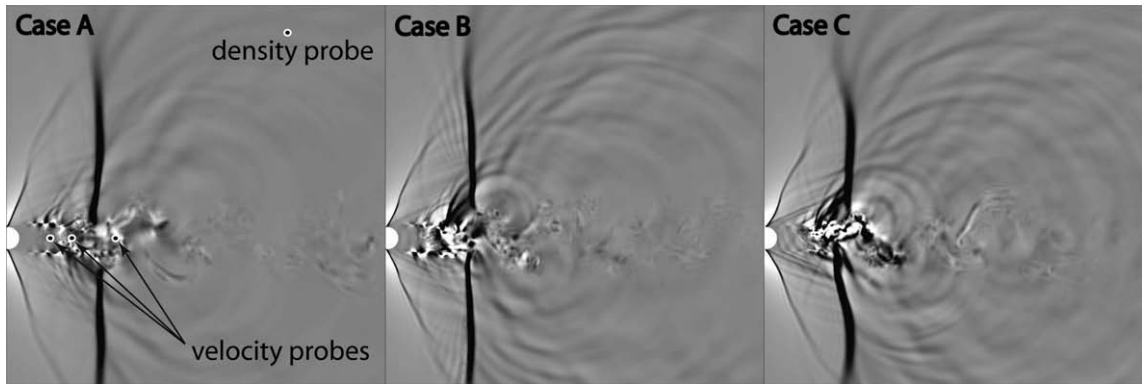


Fig. 3. Instantaneous dilatation fields for the different methods in Table 1, with contour levels between $\pm 0.5c_\infty/D$. A density probe at $(x, y) = (12.9D, 9.3D)$ is employed to compare the far-field sound of the different simulations. Three velocity probes are employed to compare the turbulent velocity spectra in the wake center-line. These probes are located at $x = 2D, 3D$, and $5D$, respectively, corresponding to the transition region, pre-shock, and post-shock turbulent wake. The origin of the coordinate system is at the center of the cylinder.

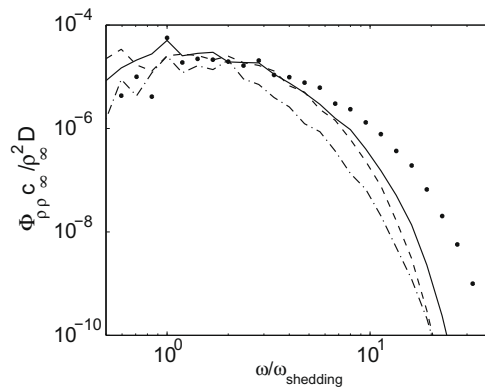


Fig. 4. Far-field sound spectra (density) computed at $(x, y) = (12.9D, 9.3D)$ for Case A (dashdotted), Case B (solid), and Case C (dashed). The symbols represent in fine-grid result.

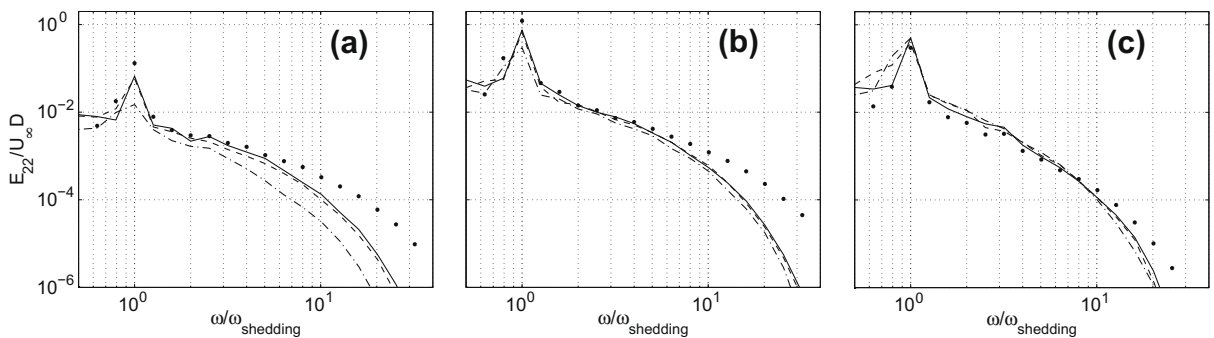


Fig. 5. Spectra of vertical velocity fluctuations along the symmetry axis at $x = 2D$ (a), $x = 3D$ (b), and $x = 5D$ (c), with line styles as in Fig. 4. The spectra are averaged in the spanwise direction and bin-averaged over $1/3$ octave. A Hanning window is used to remove the frequency leakage.

This underprediction in the velocity spectrum can lead to a significant difference on measurable integral quantities. For example, the fluctuations of the lift coefficient are underpredicted due to an excess of ABV in Case A as shown in Table 2. This is expected since the lift coefficient is closely related to vertical velocity fluctuations in the near wake. Note that the fluctuating lift coefficient for this flow is significantly smaller than that of subsonic flows, and is apparently very challenging to compute.

Table 2

Integral quantities obtained with different ABV methods, with estimated statistical errors due to convergence of the averages.

	Case A	Case B	Case C	Refined
C_D	1.44 ± 0.05	1.49 ± 0.03	1.48 ± 0.04	1.53 ± 0.02
$C_{l,rms}$	0.0075 ± 0.0025	0.011 ± 0.002	0.011 ± 0.002	0.016 ± 0.002

Both the lift coefficient and the velocity spectra are the same in Cases B and C. This again indicates that most of the model improvement can be achieved by replacing S with $\nabla \cdot \mathbf{u}$ in the formulation, while further changes make little impact.

4. Conclusions

We used a combination of standard LES subgrid scale eddy viscosity model and the artificial bulk viscosity method to simulate turbulent flow over a circular cylinder at Reynolds number of 10,000 and Mach number of 0.85. The excessive ABV introduced by the Cook and Cabot model was found to overly damp the sound field and affect integral quantities such as the lift coefficient. An alternative formulation that is parameterized by dilatation, rather than strain-rate magnitude, was shown to be localized more effectively around shocks and provide a less intrusive shock-capturing treatment. This modification was shown to improve the capabilities of LES+ABV in predicting sound and transition. In addition, flow statistics such as velocity spectra, lift, and drag coefficient were found to be insensitive to model parameters (order r) after the proposed modifications. The high order formulation was found to be necessary for the prediction of sound propagation, and it is recommended that $r \geq 1$ is used.

In addition, we propose (in Appendix A) an extension of the method to general curvilinear grids that ensures consistent shock capturing regardless of alignment (or lack thereof) between the shock and the grid. This modification allows for stable computations of the flow around a cylinder, where the grid is highly skewed in the regions of the strongest shocks.

Acknowledgments

This work has been supported by the Air Force Office of Scientific Research under grant no. FA9550-06-1-0147 and the DOE SciDAC program. Ali Mani is supported by a Charles H. Kruger Stanford Graduate Fellowship. Computer time was provided by NAS at NASA Ames Research Center.

Appendix A. Extension to curvilinear grids

This Appendix defines the operator $D^{2r}(\cdot)$ which mimics $\Delta^{(2r+2)}\nabla^{2r}(\cdot)$ on curvilinear grids in multiple dimensions. Cook and Cabot [4] suggested using the cube-root of the volume element as the length scale Δ in multiple dimensions, which works reasonably for nearly isotropic grids. They used successive Laplacians to bias β_A towards high wavenumbers, which leads to tensorial invariance. We note that tensorial invariance is not a requirement in the present work since the discretized space is already anisotropic; furthermore, in the continuum limit (fine grid) β_A is zero and will not affect the invariance of the governing equations. The ABV method should only thicken shocks such that they can be resolved on the given grid. To extend the ABV concept to higher dimensions (on anisotropic grids) we consider the following consistency criteria:

- (1) β_A should not depend on the lab coordinate and its orientation.
- (2) If a shock is aligned with a grid line (in 2D) or grid plane (in 3D), then β_A should be identical to its 1D value.

The method by Cook and Cabot [4] and the extension in Ref. [5] do not satisfy the second criterion. Consider Fig. 6 which shows a curvilinear mesh defined by coordinates ξ and η . At each point, the vectors $\Delta\xi$ and $\Delta\eta$ define the displacement towards the next ξ and η point, respectively. A simple curvilinear definition of $D^{2r}(\cdot)$ is (in 2D for simplicity; the 3D definition follows trivially)

$$D^{2r}(\cdot) = \Delta_1^2 \left| \frac{\partial^{2r}(\cdot)}{\partial \xi^{2r}} \right| + \Delta_2^2 \left| \frac{\partial^{2r}(\cdot)}{\partial \eta^{2r}} \right|, \tag{3}$$

where Δ_1 and Δ_2 are two resolution length scales. Since the curvilinear coordinates are non-dimensional, there is no need for an additional Δ^{2r} factor in the equation. A simple choice for the length scales Δ_1 and Δ_2 could be $|\Delta\xi|$ and $|\Delta\eta|$, respectively (essentially the choice of Ref. [5]). However, this choice does not satisfy the second criterion above. For example, Fig. 6 shows a case where the shock is aligned with constant ξ lines. In this case the flow is 1D (function of ξ only), and our second criterion implies that the correct resolution length scale is the Δ_{res} in the figure. Having made these observations, we define the resolution length scales in Eq. (3) as

$$\Delta_1 = \Delta\xi \cdot \frac{\nabla\rho}{|\nabla\rho|}, \quad \Delta_2 = \Delta\eta \cdot \frac{\nabla\rho}{|\nabla\rho|}. \tag{4}$$

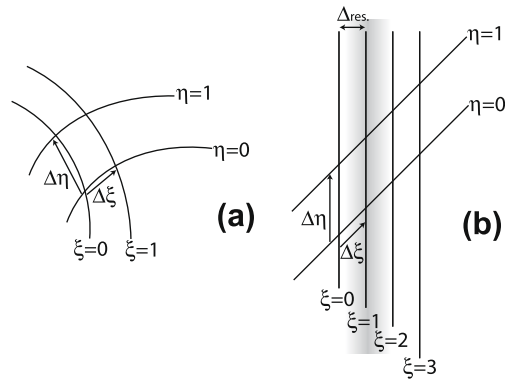


Fig. 6. Schematics of a general curvilinear mesh (a), and a special case where the shock is aligned with the grid-lines of constant ξ on a highly skewed mesh (b).

In other words, the grid spacing projected in the shock normal direction ($\nabla\rho/|\nabla\rho|$) is used as the length scale. We note that Eqs. (3) and (4) are not the only possible curvilinear extensions which satisfy the aforementioned criteria; however, we adopted this formulation for our computations.

References

- [1] R. Mittal, P. Moin, Suitability of upwind-biased finite difference schemes for large-eddy simulation of turbulent flows, *AIAA J.* 35 (8) (1997) 1415–1417.
- [2] J. Larsson, S.K. Lele, P. Moin, Effect of numerical dissipation on the predicted spectra for compressible turbulence, in: *Annual Research Briefs, Center for Turbulence Research*, 2007, pp. 47–57.
- [3] J.V. Shebalin, Pseudospectral simulation of compressible turbulence using logarithmic variables, *AIAA Paper* 93-3375.
- [4] A.W. Cook, W.H. Cabot, Hyperviscosity for shock-turbulence interactions, *J. Comput. Phys.* 203 (2005) 379–385.
- [5] S. Kawai, S.K. Lele, Localized artificial diffusivity scheme for discontinuity capturing on curvilinear meshes, *J. Comput. Phys.* 227 (2008) 9498–9526.
- [6] P. Moin, K. Squires, W. Cabot, S. Lee, A dynamic subgrid-scale model for compressible turbulence and scalar transport, *Phys. Fluids* 3 (11) (1991) 2746–2757.
- [7] D.K. Lilly, A proposed modification of the Germano subgrid-scale closure method, *Phys. Fluids* 4 (3) (1992) 633–635.
- [8] S. Nagarajan, S.K. Lele, J.H. Ferziger, A robust high-order compact method for large eddy simulation, *J. Comput. Phys.* 191 (2003) 392–419.
- [9] A. Mani, P. Moin, M. Wang, Computational study of optical distortions by separated shear layers and turbulent wakes, *J. Fluid Mech.* 625 (2009) 273–293.